PROBING LARGE WAVEVECTOR PHONONS AT THE NANOSCALE VIA X-RAY THERMAL DIFFUSE SCATTERING

Gokul Gopalakrishnan[1], Martin V. Holt[2], Kyle M. McElhinny[1], David A. Czaplewski[2], Paul G. Evans[1]

[1] Materials Science and Engineering and Materials Science Program, University of Wisconsin, Madison, WI 53706, USA

[2] Center for Nanoscale Materials, Argonne National Laboratory, Argonne, IL 60439, USA

ABSTRACT

The ability to engineer the thermal properties of materials using nanotechnology has seen a recent series of rapid advances. Experimental probes for phonons with large wavevectors have been largely based on inelastic x-ray and neutron scattering. The signals of inelastic scattering techniques become impractically weak in small ensembles of nanoscale objects, which pose severe constraints on their applications to materials with nanoscale dimensions. Advances in high brilliance x-ray sources at synchrotron facilities have revived interest in thermal diffuse scattering (TDS), which is an energy-integrated analog of the inelastic techniques. We demonstrate that TDS can be extended from its widespread use in macroscopic samples to nanoscale systems. We describe results of x-ray TDS measurements performed on suspended silicon nanomembranes, and show that this approach allows the range of wavevectors probed in these systems to extend far from the zone center. Edge-supported Si membranes with thicknesses as small as a few tens of nanometers were fabricated by releasing the device layer of a silicon-on-insulator structure. Experiments were conducted using a 30 μm-diameter focused beam of X-rays with a photon energy of 10 keV. The scattering geometry was selected so that the TDS signal was collected over a slice of reciprocal space corresponding to phonon momenta extending from near the center of the Brillouin zone to the zone boundaries. The scattered X-ray intensity distributions provide information about the populations of acoustic phonons spanning the entire Brillouin zone in Si nanomembranes.

This document was presented at the Denver X-ray Conference (DXC) on Applications of X-ray Analysis.

Sponsored by the International Centre for Diffraction Data (ICDD).

This document is provided by ICDD in cooperation with the authors and presenters of the DXC for the express purpose of educating the scientific community.

Usage is restricted for the purposes of education and scientific research.

DXC Website
– www.dxcicdd.com

ICDD Website
- www.icdd.com

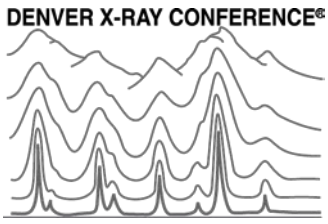

I. INTRODUCTION

Inelastic X-ray and neutron scattering have long been used to probe phonon modes in macroscopic samples (Delaire *et al.*, 2011; Nilsson and Nelin, 1972; Saviot *et al.*, 2008; Schwoerer-Bohning *et al.*, 1998). Small scattering cross sections and stringent photon-energy resolution requirements, however, render inelastic techniques unsuitable for sample volumes smaller than approximately 1000 μm^3(Dennis and Webb, 1973; Reichert *et al.*, 2007). Within this inaccessible volume regime, however, the phonon dispersion of nanoscale structures is predicted to be strongly modified by the presence of boundaries separated by length scales comparable to the phonon wavelength (Lamb, 1917; Mindlin and Medick, 1959; Schwab *et al.*, 2001). The preferred techniques for nanoscale systems are Raman and Brillouin scattering (Cuffe *et al.*, 2012; Groenen *et al.*, 2008; Torres *et al.*, 2004), which are sensitive to small-wavevector acoustic and optical phonons residing at the zone center, but possess a fundamental mismatch with the wavelengths of the majority of phonons modes, spanning the rest of the Brillouin zone. These large-wavevector phonons influence thermal transport in nanomaterials because longer-wavelength phonons are more effectively scattered by boundaries and interfaces (Ju and Goodson, 1997; Liu and Asheghi, 2006). Phonon engineering at the nanoscale has been, in some sense, limited by a lack of probes that combine sufficient momentum range to probe entire phonon dispersion with sufficiently strong signals to study nanoscale structures. We address this problem by demonstrating the potential to probe large-wavevector phonons in single-crystal silicon nanomembranes using synchrotron X-ray thermal diffuse scattering (TDS). We apply this technique to sample volumes as small as 10 μm^3.

TDS is an energy-integrated analog of inelastic scattering, and is particularly sensitive to the large density of thermally populated low energy acoustic phonons (Holt *et al.*, 1999). Although TDS has been previously used to map phonon dispersions and to study phase transitions, these experiments have all been restricted to bulk systems (Colella and Batterman, 1970; Holt *et al.*, 2007; Holt *et al.*, 1999; Holt *et al.*, 2001). Holt *et al*. (1999) describe, for example, a procedure to determine the phonon dispersion for bulk silicon from TDS images obtained with exposure times of only a few seconds. The high X-ray fluxes available synchrotron light sources and the

simultaneously small beam sizes achieved at nanoprobe facilities have created the opportunity to use TDS as a probe of phonons in nanostructure assemblies, bridging the gap between the capabilities of bulk techniques like neutron scattering and those of small wavevector optical scattering probes.

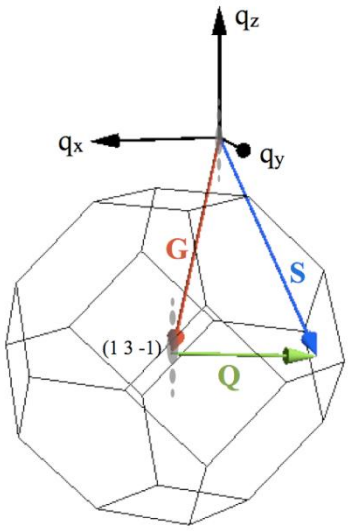

Figure 1. The intensity arising from first-order TDS at a scattering wavevector **S** is due to phonons with wave vector **Q**, where **S**=**G**+**Q** and **G** is the reciprocal lattice vector of the nearest reciprocal lattice vector. The finite thickness of membranes elongates Bragg reflections into rods normal to the thickness direction. In the geometry chosen for this experiment, the detector captures intensity scattered into the first Brillouin zone around the (1 3 -1) point in the reciprocal lattice.

In a bulk single crystal at temperature *T*, the first-order TDS intensity from the scattering of an unpolarized beam by a phonon of wavevector **Q** is given by:

$$I(\boldsymbol{Q}) \propto f^2 e^{-2M} \sum_{j=1}^{6} \frac{\left|\boldsymbol{Q}\cdot\hat{\boldsymbol{e}}_j\right|^2}{\omega_j} \coth\left(\frac{\hbar\omega_j}{2k_B T}\right)$$

where *f* is the atomic scattering factor, *M* is the Debye-Waller factor, ω_j and $\mathbf{e_j}$ are respectively the frequency and polarization of the jth phonon branch (Holt *et al.*, 1999). The intensity recorded by the detector for a reciprocal space scattering vector **S** is determined by phonons with wavevector **Q**, where **Q** is the difference between **S** and the nearest reciprocal lattice point **G**, as

shown in Fig 1. For modes with $\hbar\omega << k_BT$, the TDS intensity scales approximately as $1/\omega^2$. With the absence of competing elastic scattering processes under these conditions, TDS becomes particularly sensitive to the dispersion, $\omega(\mathbf{Q})$, of low-energy acoustic phonons (Holt *et al.*, 2007; Holt *et al.*, 2001).

II. EXPERIMENTAL

TDS experiments on nanomembrane samples were performed in a transmission geometry at station 26-ID-C of the Advanced Photon Source (APS) at Argonne National Laboratory (Fig. 2). Samples were mounted normal to the incident beam in an evacuated chamber, in order to minimize the contribution of X-ray scattering by air. A 10-keV X-ray beam was focused onto the membrane by a capillary condenser resulting in an X-ray spot diameter of 30 μm. Unfocused and secondary X rays from upstream sources were eliminated using a 30 μm-diameter order sorting aperture located between the condenser and the sample. A Pb beam stop was positioned downstream from the sample to absorb the transmitted direct beam. Lead shielding was shaped into a truncated pyramid extending from the beryllium exit window of the evacuated chamber to the sample. The shielding was positioned in the chamber to prevent scattering from optics and other surfaces inside the chamber from reaching the detector. X rays scattered by the sample were detected using a charge-coupled device (CCD) (Mar Inc.) with a pixel size of 80 μm and a total diameter of 165 mm. The detector subtended an angle of approximately 15°. The sample orientation was chosen to avoid exciting Bragg reflections and to capture the TDS signal from wavevectors ranging from about $0.1(2\pi/a)$, representing points near the zone center, to $2\pi/a$, corresponding to points on the zone edges. Here a is the Si lattice parameter, 0.543 nm.

TDS intensity distributions for a series of samples were collected from the bulk Si supports as well as from the suspended Si membranes. An additional set of background measurements, nominally with no sample at all, were recorded by directing the incident beam through an opening in the sample where one of the membranes was mechanically removed. These background images allowed the sources of scattering outside the sample to be subtracted from the sample images to obtain an accurate measurement of the TDS intensity. Each set of measurements consisted of repetitions of a pair of 300-s exposures that were double-correlated to

eliminate zingers, random events from cosmic rays or from radioactive decay of isotopes within the detector. Averaged images from a series of scans with a cumulative exposure time of approximately 1 hour were required to resolve the weak TDS signal from phonons near the zone boundaries. The experimentally observed TDS intensity from the membranes was compared with calculated intensity distributions and with experimental observations of TDS from bulk Si.

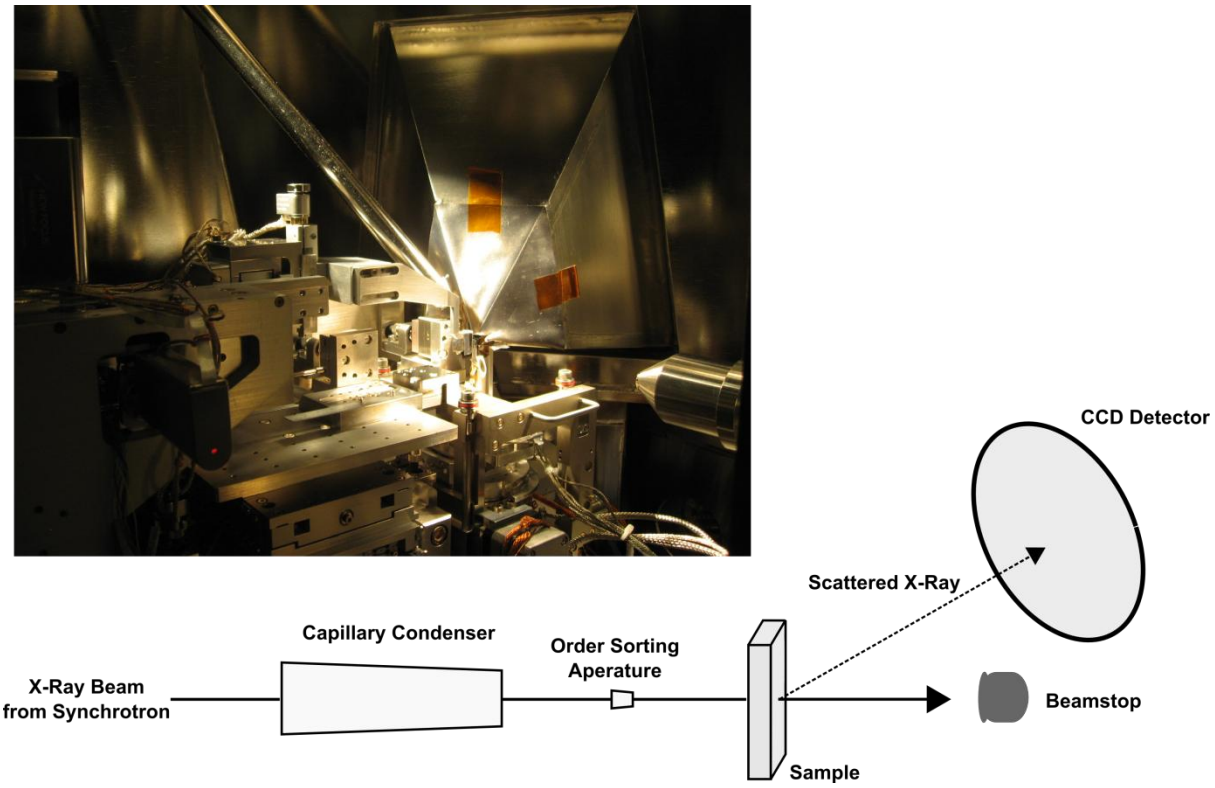

Figure 2. Schematic and photograph of the experimental arrangement for these measurements at station 26-ID-C of the Advanced Photon Source (APS). The measurement was performed in vacuum to eliminate contributions to the measured intensity due to scattering from air.

Figure 3 shows a single detector image of TDS from a bulk region of the sample. The experiment was designed so that the detector collected the intensity in a slice in which the closest reciprocal lattice point was (1 3 -1). The intersection of the Ewald sphere with boundaries of the region of reciprocal space that is closer to (1 3 -1) than to any other reciprocal lattice point are overlaid on the detector image. Relatively high TDS intensities are observed near the zone center, because of the large thermal occupancy of small-wavevector phonons. A diagonal streak of intensity

extends along a direction close to [100], from near the zone center towards the X-point on the edge of the Si Brillouin zone.

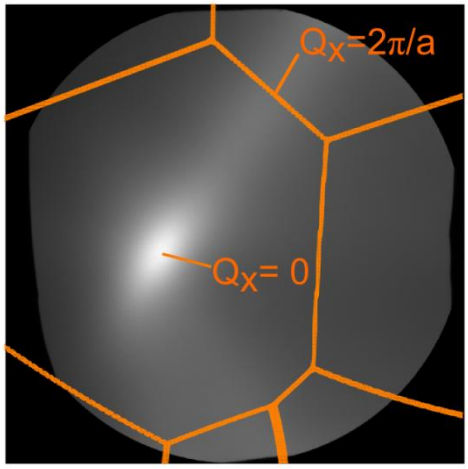

Figure 3. TDS intensity distribution from bulk silicon. The boundaries of the Brillouin zones are shown as orange lines. The detector image spans an angular range of approximately 15° in each dimension.

Our initial TDS measurements on Si nanomembranes revealed an undesirable effect arising from the static distortion of the lattice due to strain induced buckling of the membranes. As a result, the process used to fabricate the membranes was redesigned to eliminate the buckling. Before this modification, the process began with silicon-on-insulator (SOI) structures with a device layer of submicron thickness on a buried oxide (BOX) layer, supported by a handle wafer with a thickness of 625 μm. The device layer of the SOI was first thinned down to the desired thickness by etching in TMAH. Using low stress silicon nitride (SiN) as an etch mask, the handle wafer was patterned and etched in KOH, with the BOX layer serving as an etch stop. Removing the buried oxide in 49% HF solution released square membrane windows measuring about 200 μm along the edge. This procedure produced membranes which were buckled in response to biaxial stresses built into the device layer during the fabrication of the parent SOI structure. Such buckling has been previously observed in nanomembranes fabricated from SOI (Torres *et al.*, 2004) and presents a significant technical hurdle for experiments and applications requiring single crystal nanomembrane structures.

We used two different modifications of the fabrication process to overcome the buckling problem. With the first approach, we patterned long strain relief arms connecting the suspended membrane to the rest of the sample. These narrow arms concentrated the majority of the elastic deformation away from the central region of the membrane, reducing the extent of buckling within it. The second approach involved the flattening of the membranes via a low-energy intermediate structure utilizing the surface energy of the Si-water interface. In this scheme, the selective HF etch of the BOX layer was performed so as to undercut the device layer by 30 μm, creating a shelf on the underlying Si handle wafer. A final wetting-dewetting step in DI water adhered the near-edge regions of the released membrane to this shelf, resulting in flat, single crystal membranes. The second approach is described in detail in a separate publication (Gopalakrishnan *et al*., Submitted).

III. RESULTS

TDS images of the Brillouin zone centered on the (1 3 -1) reciprocal lattice point were captured from buckled membranes as well as from the flattened membranes fabricated by the two procedures described above. Figure 4 shows a comparison of detector images from a buckled 67-nm membrane, a 70-nm membrane suspended from strain relief arms, and a 44-nm membrane fabricated by undercutting the BOX. The dominant contribution to the scattering pattern observed with the buckled membrane [Fig. 4(A)] arises from the static strain field resulting from the buckling. The TDS from the 70-nm strain relieved membrane [Fig 4(B)] shows significant improvement, with TDS signals similar to those of bulk Si. Fig. 4(B) still reveals, however, some drawbacks of the fabrication based on strain-relief arms. The low stiffness of the arms allows the membrane to change its orientation slightly over the course of several minutes. The variation in the orientation of the membrane causes the TDS intensity distribution to move to a series of new positions on the detector during a long set of exposures. This is most clearly visible in the large angular distribution of the intensity associated with the crystal truncation rod, located near the left edge of the detector image. Furthermore, the orientation of the membrane supported by flexible arms is different than the bulk handle wafer because of the low stiffness of the arms. As a result, direct comparisons of bulk and membrane TDS from the sample with the strain relief arms are difficult.

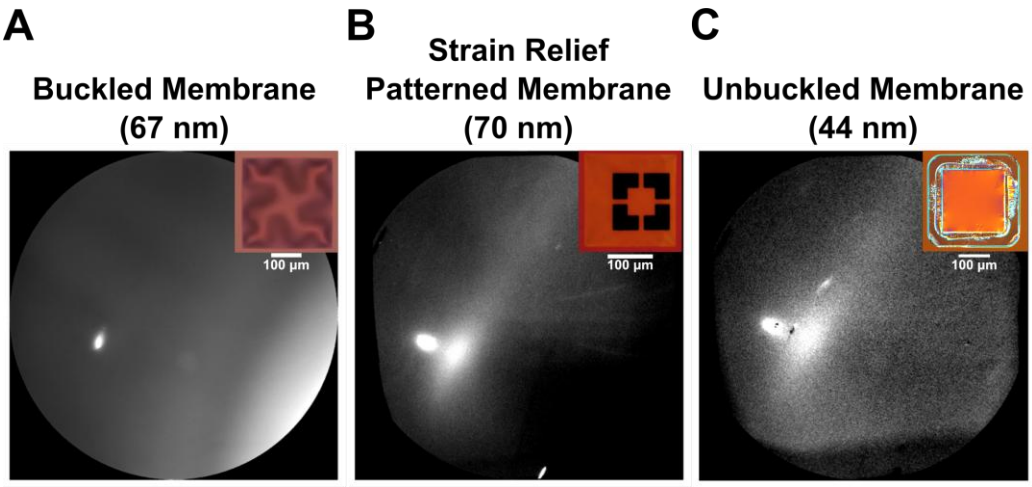

Figure 4. TDS intensity distributions from (A) a buckled 67-nm thick membrane, (B) a strain-relieved 70-nm thick membrane, and (C) a flat 44-nm membrane. Optical micrographs of each membrane are inset in the scattering patterns. The crystal truncation rod of the membrane appears as the sharp region of high intensity near the left edge of each image. The TDS observed with the flat membrane in (B) and (C) is overwhelmed in (A) by scattering from the strain field of the buckled membrane. The truncation rod in (B) is spread due to sample motion during the measurement.

TDS images were also obtained from flat membranes fabricated by the undercut etching process [Fig 4(C)]. The intensity distribution in Fig. 4(C) reveals a minimal contribution from static distortion of the membrane. Deviations from flatness were measured by white light interferometry (Zygo NewView) and typically found to be less than 20 nm across a central region spanning over 100 μm in extent. TDS images obtained from thick membranes closely match the distribution calculated from bulk Si.

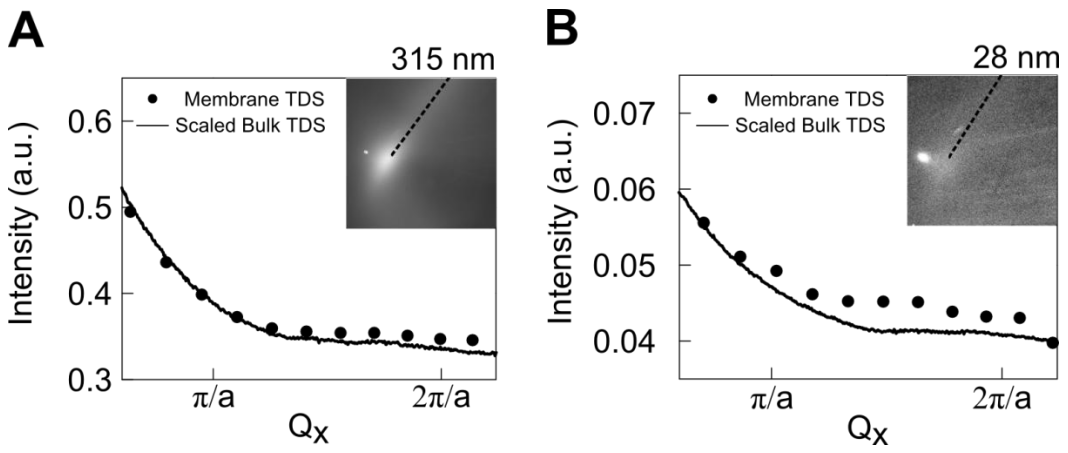

Figure 5. Line profiles of the TDS intensity distribution from (A) a 315-nm thick membrane and (B) a 28-nm thick membrane. The dots represent the measured intensity from the membrane. The solid lines are measurements from the bulk regions of the same samples, scaled to match a least squares fit to the membrane TDS. The horizontal axis is the x-component of the phonon wavevector. The detector images from which the line profiles are drawn are inset in each plot. Dashed lines indicate the path along which the profiles are plotted.

Deviations from bulk behavior are observed in thinner membranes. Fig 5 shows the detector images from (A) a flat 315-nm membrane and (B) a flat 28-nm membrane, fabricated by the undercut etch. Line profiles (dotted curve) were extracted along the dashed line, indicated in the inset, passing through the diagonal TDS streak extending towards the Si X-point. The solid lines are from measurements in the bulk regions of the same samples. The bulk profiles have each been multiplied by a single scaling parameter, to best fit the membrane TDS profile. The TDS intensities in these profiles are plotted as a function of the x-component of the phonon wavevector. Deviations from the TDS measured in bulk Si are observed at large wavevectors in the 28-nm membrane. Systematic deviations in this range of wavevectors for nanomembranes with thicknesses in the tens of nm are not well explained by the scattering contribution from native oxide or from strain in the membrane. They are consistent, however, with a softening of phonons modes in nanomembranes by a modification of the boundary conditions from that of the bulk. Bannov *et al*. (1995) present an elastic continuum model calculation for the dispersion of vibrational modes in a free-standing quantum well. Using this calculation for unsupported Si nanomembranes reveals that energies of the lowest modes are smaller than those of the lowest modes in bulk Si.

IV. CONCLUSION

Synchrotron X-ray TDS measurements allow the description of phonons in scientifically and technologically important Si nanostructures to move beyond the low-wavevector models commonly used for such systems. This technique will furthermore allow large-wave-vector acoustic phonons to be probed at the nanoscale in other crystalline materials where phonons determine phase transformations and thermal transport phenomena, and for which experimental insight is currently available only in bulk samples (Balandin and Wang, 1998; Cahill *et al.*, 2003). Further advances in X-ray nanobeam techniques promise to allow TDS to become a powerful tool for probing phonons in individual nanostructures and studying dynamics at the nanoscale (Ice *et al.*, 2011).

ACKNOWLEDGMENTS

GG, KM, and PE acknowledge support from the US Air Force Office of Scientific Research (contract FA9550-10-1-0249). MH and DC, as part of the Center for Nanoscale Materials core research program, and use of the Advanced Photon Source were supported by the U. S. Department of Energy, Office of Science, Office of Basic Energy Sciences (contract no. DE-AC02-06CH11357). The authors gratefully acknowledge Dr. Ralu Divan, at the Center for Nanoscale Materials, and Dr. Rob Ilic, at the Cornell Nanoscale Science and Technology Facility, for assistance with device fabrication. Fabrication was performed at the Wisconsin Center for Applied Microelectronics, at the University of Wisconsin, in Madison, and at the Center for Nanoscale Materials at Argonne National Laboratory.

REFERENCES

Balandin, A. and Wang, K. L. (**1998**). "Significant decrease of the lattice thermal conductivity due to phonon confinement in a free-standing semiconductor quantum well," Phys. Rev. B **58**, 1544-1549.

Bannov, N., Aristov, V., Mitin, V. and Stroscio, M. A. (**1995**). "Electron relaxation times due to the deformation-potential interaction of electrons with confined acoustic phonons in a free-standing quantum well," Phys. Rev. B **51**, 9930-9942.

Cahill, D. G., Ford, W. K., Goodson, K. E., Mahan, G. D., Majumdar, A., Maris, H. J., Merlin, R. and Phillpot, Sr. (**2003**). "Nanoscale thermal transport," J. Appl. Phys. **93**, 793-818.

Colella, R. and Batterman, B. W. (**1970**). "X-ray determination of phonon dispersion in vanadium," Phys. Rev. B **1**, 3913.

Cuffe, J., Chavez, E., Shchepetov, A., Chapuis, P.-O., El Boudouti, E. H., Alzina, F., Kehoe, T., Gomis-Bresco, J., Dudek, D., Pennec, Y., Djafari-Rouhani, B., Prunnila, M., Ahopelto, J. and Sotomayor Torres, C. M. (**2012**). "Phonons in slow motion: Dispersion relations in ultrathin si membranes," Nano Lett. **12**, 3569-3573.

Delaire, O., Ma, J., Marty, K., May, A. F., Mcguire, M. A., Du, M. H., Singh, D. J., Podlesnyak, A., Ehlers, G., Lumsden, M. D. and Sales, B. C. (**2011**). "Giant anharmonic phonon scattering in PbTe," Nature Mater. **10**, 614–619.

Dennis, R. L. and Webb, M. B. (**1973**). "Thermal diffuse scattering of low-energy electrons at low-temperature," J. Vac. Sci. Technol. **10**, 192-195.

Gopalakrishnan, G., Czaplewski, D. A., McElhinny, K. M., Holt, M. V., Silva-Martinez, J. C., Evans, P. G. (Submitted). "Edge-induced flattening in the fabrication of ultrathin free-standing crystalline silicon sheets," Appl. Phys. Lett.

Groenen, J., Poinsotte, F., Zwick, A., Torres, C., Prunnila, M. and Ahopelto, J. (**2008**). "Inelastic light scattering by longitudinal acoustic phonons in thin silicon layers: From membranes to silicon-on-insulator structures," Phys. Rev. B **77**, 045420.

Holt, M., Sutton, M., Zschack, P., Hong, H. and Chiang, T. (**2007**). "Dynamic fluctuations and static speckle in critical X-ray scattering from SrTiO3," Phys. Rev. Lett. **98**, 065501.

Holt, M., Wu, Z., Hong, H. W., Zschack, P., Jemian, P., Tischler, J., Chen, H. and Chiang, T. C. (**1999**). "Determination of phonon dispersions from X-ray transmission scattering: The example of silicon," Phys. Rev. Lett. **83**, 3317-3319.

Holt, M., Zschack, P., Hong, H., Chou, M. and Chiang, T. (**2001**). "X-ray studies of phonon softening in $TiSe_2$," Phys. Rev. Lett. **86**, 3799-3802.

Ice, G. E., Budai, J. D. and Pang, J. W. L. (**2011**). "The race to X-ray microbeam and nanobeam science," Science **334**, 1234-1239.

Ju, Y. S. and Goodson, K. E. (**1997**). "Size effect on thermal conduction in silicon-on-insulator devices under electrostatic discharge (esd) conditions," Japan. J. Appl. Phys. Pt. 2 - Lett. **36**, L798-L800.

Lamb, H. (**1917**). "On waves in an elastic plate," Proc. Roy. Soc. A **93**, 114-128.

Liu, W. J. and Asheghi, M. (**2006**). "Thermal conductivity measurements of ultra-thin single crystal silicon layers." J. Heat Transf. - Trans. ASME **128**, 75-83.

Mindlin, R. D. and Medick, M. A. (**1959**). "Extensional vibrations in elastic plates," J. Appl. Mech. **26**, 561-569.

Nilsson, G. and Nelin, G. (**1972**). "Study of homology between silicon and germanium by thermal-neutron spectrometry," Phys. Rev. B **6**, 3777.

Reichert, H., Bencivenga, F., Wehinger, B., Krisch, M., Sette, F. and Dosch, H. (**2007**). "High-frequency subsurface and bulk dynamics of liquid indium," Phys. Rev. Lett. **98**, 096104.

Saviot, L., Netting, C. H., Murray, D. B., Rols, S., Mermet, A., Papa, A.-L., Pighini, C., Aymes, D. and Millot, N. (**2008**). "Inelastic neutron scattering due to acoustic vibrations confined in nanoparticles: Theory and experiment," Phys. Rev. B **78**, 245426.

Schwab, K., Arlett, J. L., Worlock, J. M. and Roukes, M. L. (**2001**). "Thermal conductance through discrete quantum channels," Physica E **9**, 60-68.

Schwoerer-Bohning, M., Macrander, A. T. and Arms, D. A. (**1998**). "Phonon dispersion of diamond measured by inelastic X-ray scattering," Phys. Rev. Lett. **80**, 5572-5575.

Torres, C. M. S., Zwick, A., Poinsotte, F., Groenen, J., Prunnila, M., Ahopelto, J., Mlayah, A. and Paillard, V. (**2004**). "Observations of confined acoustic phonons in silicon membranes," physica status solidi (c) **1**, 2609-2612.